Pion structure from improved lattice QCD: Form factor and charge radius at low masses

J. van der Heide*

National Institute for Nuclear Physics and High-Energy Physics (NIKHEF), 1009 DB Amsterdam, The Netherlands

J. H. Koch[†]

NIKHEF and Institute for Theoretical Physics, University of Amsterdam, Valckenierstraat 65, 1018 XE Amsterdam, The Netherlands

E. Laermann[‡]

Fakultät für Physik, Universität Bielefeld, D-33615 Bielefeld, Germany

The charge form factor of the pion is calculated in lattice QCD. The nonperturbatively improved Sheikholeslami-Wohlert action is used together with the $O(a)$ improved vector current. Other choices for the current are examined. The form factor is extracted for pion masses from 970 down to 360 MeV and for momentum transfers $Q^2 \leq 2 \, \text{GeV}^2$. The mean square charge radius is extracted and compared to previous determinations, and its extrapolation to lower masses discussed.

I. INTRODUCTION

QCD without doubt is the correct microscopic theory describing all strong interactions, a fact that has been established mainly by impressive agreement between theory and experiment in the perturbative sector. Comparatively few results have been obtained in nonperturbative QCD, which deals with physics on the scale of Λ_{QCD} or the size of a hadron. It is therefore an obvious challenge to derive the internal structure of a hadron from first principles, entirely within QCD [1]. Next to the nucleon, the pion is an obvious candidate for such an attempt. Its global features, like charge, spin, and isospin, represent no challenge and are trivially included in any model. Specific features that actually test details of our theoretical understanding are observables like the pion form factor and its polarizability. In this paper, we report on an extensive study of the pion form factor based on lattice QCD. The first results were already reported in [2,3].

At first glance, the pion looks like a manageable two-body system, and there have been many descriptions of the pion based on effective models or QCD inspired approaches. One feature all these attempts share is that confinement, the most striking feature of QCD, is—in one way or another—put in by hand. This is of course an unwanted step when one sets out to calculate the pion form factor or its mean square charge radius, which reflect the form and size of QCD confinement. Here one obviously wants to proceed from first principles, from the fundamental QCD Lagrangian itself.

Several papers have already dealt with aspects of the pion structure in lattice QCD. A quantity often considered is the "Bethe-Salpeter amplitude," the relative quark-antiquark wave function, extracted from two-point functions [4–7]. Another approach is based on gauge invariant density-density correlations [1,7,8], most recently by Alexandrou

et al. [9]. Two groups have already calculated the pion charge form factor, proceeding, as in the present work, in the quenched approximation. The pioneering work was done by Martinelli and Sachrajda [10], followed by more detailed calculations of Draper *et al.* [11]. One of the findings of the latter work was that the pion form factor could be described quite well by a monopole form, as suggested by vector meson dominance. As shown in [2], the range parameter is in fact very close to the ρ mass obtained for the same action.

Lattice calculations, although starting from first principles, are not free of approximations. The most obvious one is the use of the lattice itself, necessarily resulting in discretization errors. These errors can be reduced by the use of improved lattice QCD actions and the concomitant improved observables. In the work reported here, we extend the previous work by working in $O(a)$ improved lattice QCD, which guarantees that errors in the matrix elements we extract are only of order $O(a^2)$. In order to emphasize the importance of consistently using both improved action and observables, we discuss the form of the vector current operator at some length and give numerical examples for the results one obtains with the current operators used in other work.

In addition to the step from a discrete lattice to the physical continuum, one also has to extrapolate the lattice results in the pion mass. As is known, lattice calculations yield results for pions much heavier than the physical pion. The previous form factor calculations in [10,11] were for pions on the order of 1 GeV. Another improvement step which we undertake in this paper is to extend our calculations of the electric form factor down to pion masses of 360 MeV. For the mean square charge radius of the pion which we extract from the form factor, we then study the extrapolation to lower masses.

It is instructive to compare the mean square radii obtained from the Bethe-Salpeter amplitudes and from the form factor. We find considerable differences which, as suggested earlier [6], can be ascribed to the effect of the gluon motion on the position of the center of mass.

The paper is organized as follows. In Sec. II, we first

---

*Electronic address: r86@nikhef.nl

[†]Electronic address: justus@nikhef.nl

[‡]Electronic address: edwin@physik.uni-bielefeld.de

FIG. 1. Two-point function.

describe the general features of our approach and the details of our lattice calculations. Results for the two- and three-point function are described in Secs. III and IV, respectively. Our findings for the form factor and the mean square radius of the pion are elaborated in Sec. V. A summary of our work and conclusions are contained in Sec. VI.

II. THE GENERAL METHOD

A. The observables

To obtain the pion form factor from the lattice, one has to calculate two observables, the two- and three-point Green's functions for an interacting quark-antiquark pair with the quantum numbers of the pion. Improved techniques are used in order to remove $O(a)$ discretization effects. We do this nonperturbatively for both the action and the electromagnetic vector current in the three-point function. Fits to both observables were used to extract the desired information, such as the form factor and the pion mass.

The two-point function, shown schematically in Fig. 1, projected to momentum $\mathbf{p}$ is given by

$$G_{2,R}(t_f,\mathbf{p}) = \sum_{\mathbf{x}} \langle \phi_R(t_f,\mathbf{x}) \phi^\dagger(0,\mathbf{0}) \rangle e^{i\mathbf{p}\cdot\mathbf{x}}. \quad (1)$$

The operator $\phi^\dagger$ creates a quark-antiquark pair with the quantum numbers of the pion at the source at $(0, \mathbf{0})$, while $\phi(x)$ annihilates it at the sink. Since we will consider a π^+, it is given by

$$\phi^\dagger(x) = \bar{\psi}_u(x) \gamma_5 \psi_d(x). \quad (2)$$

Below, all flavor, spin, and $SU(3)$ color indices will be dropped. On the sink side, we use an extended operator with an interquark distance R. This suppresses the contribution of excited states to the two-point function and facilitates the extraction of the pion mass. In order to keep the calculation gauge invariant, the quark and antiquark at the sink are connected by gauge links. To further enhance the contribution from the pion, the links in the extended pion operator have been fuzzed to better simulate the tubelike nature of the gluon cloud.

The three-point function, shown in Fig. 2, again concerns a quark-antiquark pair with pion quantum numbers, propagating from x_i to x_f; disconnected diagrams do not contribute [1,11]. At an intermediate time t a photon is coupled to
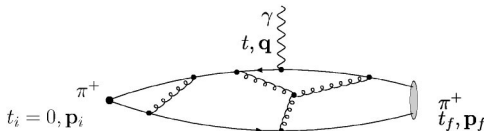
FIG. 2. Three-point function.

either one of the charged quarks. This observable is obtained in momentum space by calculating

$$G_{3,\mu}(t_f,t;\mathbf{p}_f,\mathbf{p}_i) = \sum_{\mathbf{x}_f,\mathbf{x}} \langle \phi_R(x_f) j_\mu(x) \phi^\dagger(0) \rangle$$
$$\times e^{-i\mathbf{p}_f\cdot(\mathbf{x}_f-\mathbf{x})-i\mathbf{p}_i\cdot\mathbf{x}}. \quad (3)$$

The parameter R for the pion operator at the sink is now fixed to the value giving the best overlap in the two-point function. As we will further discuss below, the choice of the current to which the quarks couple is important. The continuum or *local* current

$$j_\mu^L = \bar{\psi}(x) \gamma_\mu \psi(x) \quad (4)$$

is not conserved on the lattice and needs renormalization by a factor Z_V, yielding the *renormalized local* current j_μ^{RL}. Using the Noether procedure, one can also construct a current which is conserved on the lattice [12],

$$j_\mu^C = \bar{\psi}(x)(1-\gamma_\mu)U_\mu(x)\psi(x+\hat{\mu})$$
$$- \bar{\psi}(x+\hat{\mu})(1+\gamma_\mu)U_\mu^\dagger(x)\psi(x). \quad (5)$$

This *conserved* current still requires $O(a)$ discretization corrections for matrix elements away from the forward direction.

Using Symanzik's improvement program, one can identify appropriate operators, which, when used together with the improved action, result in matrix elements that are free of all $O(a)$ discretization errors. For the vector current considered here, the resulting *improved* current is [13–15]

$$j_\mu^I = Z_V\{j_\mu^L(x) + a c_V \partial_\nu T_{\mu\nu}\}, \quad (6)$$

with

$$T_{\mu\nu} = \bar{\psi}(x) i \sigma_{\mu\nu} \psi(x),$$

$$Z_V = Z_V^0(1+ab_V m_q). \quad (7)$$

It is conserved to $O(a^2)$ and differs from the renormalized local current by a total divergence, which vanishes for forward matrix elements. The bare quark mass is defined as

$$am_q = \frac{1}{2}\left(\frac{1}{\kappa} - \frac{1}{\kappa_c}\right), \quad (8)$$

where κ_c is the kappa value in the chiral limit and a the lattice spacing. The constants in j_μ^I are nonperturbatively determined from lattice simulations and as such completely remove the $O(a)$ effects.

From current conservation it can be shown that the general Lorentz structure of the matrix element for the electromagnetic current of an on-shell pion is

$$\langle \pi(\mathbf{p}_f)|j_\mu|\pi(\mathbf{p}_i)\rangle_{\mathrm{cont}} = (p_f + p_i)_\mu F(Q^2), \quad (9)$$
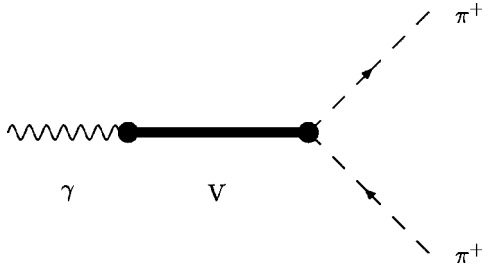
FIG. 3. The VMD model.

where $F(Q^2)$ with $Q^2 = -(p_f - p_i)^2$ is the form factor we are interested in. Connection with the continuum description is made by a proper normalization,

$$\langle\pi(\mathbf{p}_f)|j_\mu|\pi(\mathbf{p}_i)\rangle_{\text{latt}} = \frac{\langle\pi(\mathbf{p}_f)|j_\mu|\pi(\mathbf{p}_i)\rangle_{\text{cont}}}{2\sqrt{E_f E_i}}, \qquad (10)$$

where E_f and E_i are the final and initial energies, respectively.

In our calculations of the three-point function we project on initial and final three-momenta with the same length,

$$|\mathbf{p}_i| = |\mathbf{p}_f|, \qquad (11)$$

which implies that there is no energy transfer to the pion,

$$E_i = E_f. \qquad (12)$$

The four-momentum transfer to the pion, $Q^2 = (\mathbf{p}_f - \mathbf{p}_i)^2$, is then varied by changing the angle between the two momenta. Since we will use the $\mu=4$ component of the current, this choice has, among others, the numerical advantage that we have

$$\frac{E_f + E_i}{2\sqrt{E_f E_i}} = 1 \qquad (13)$$

when extracting the form factor $F(Q^2)$.

The vector meson dominance (VMD) model has been quite successful in describing both experimental as well as early lattice data. This model is inspired by effective field theory and is schematically depicted in Fig. 3. Assuming universality, i.e., $g_{\rho\pi\pi} = g_\rho$, the form factor is given by the simple monopole form

$$F(Q^2) = \left\{ 1 + \frac{Q^2}{m_V^2} \right\}^{-1}. \qquad (14)$$

B. The lattice simulation

We performed calculations in the quenched approximation on a $24^3 \times 32$ lattice. A set of 100 gluon configurations at a coupling of $\beta = 6.0$ was generated. Thermalization was reached in 2500 sweeps, whereafter we obtained configurations at intervals of 500 sweeps. One sweep consists of a pseudo-heat-bath step with FHKP updating [16] in the $SU(2)$ subgroups, followed by four over-relaxation steps.

TABLE I. Masses and $\langle r^2\rangle_{\text{BS}}$ for different k values.

κ	m_q (MeV)	m_π (MeV)	m_ρ (MeV)	$\langle r^2\rangle_{\text{BS}}$ (fm^2)
0.13230	154	970(4)	1188(6)	0.1414(2)
0.13330	101	780(4)	1053(8)	0.1480(2)
0.13380	75	670(4)	989(9)	0.1508(2)
0.13430	45	540(6)	—	0.1526(2)
0.13480	23	360(9)	—	0.1528(4)

We used the improved Sheikholeslami-Wohlert action [17] with the nonperturbatively determined [18] value of $c_{\text{SW}} = 1.769$. With this action, we computed propagators for five values of the hopping parameter corresponding to pion masses[1] of 970, 780, 670, 540, and 360 MeV; see Table I. We imposed periodic boundary conditions except in the time direction where for the fermions antiperiodic boundary conditions were implemented. The values of the constants c_V, b_V, and Z_V^0 needed to eliminate the $O(a)$ effects and to renormalize the current were taken from Bhattacharya *et al.* [20].

III. THE TWO-POINT FUNCTION

To extract physical information from the numerical data for the two-point function, Eq. (1), we use the following parametrization:

$$G_{2,R}(t_f, \mathbf{p}) = \sum_{n=0}^{1} \sqrt{Z_R^n(\mathbf{p}) Z_0^n(\mathbf{p})} e^{-E_\mathbf{p}^n N_\tau/2}$$
$$\times \cosh\left[E_\mathbf{p}^n \left(\frac{N_\tau}{2} - t_f \right) \right], \qquad (15)$$

where $N_\tau = 32$ is the extension of the lattice in the time direction. We include the contribution of the ground state ($n = 0$) with energy $E_\mathbf{p}^0$ and of the first excited state ($n = 1$) with energy $E_\mathbf{p}^1$. As discussed in connection with Eq. (1), the parameter R indicates the quark-antiquark distance at the sink, which will be chosen to enhance the contribution from the pion ground state. For this we use the approach as originally proposed in [21]. The fuzzed gluon links at the pion sink are created with a link/staple mixing of 2 and a fuzzing level of 4. The Z_R^n denote the matrix elements,

$$Z_R^n(\mathbf{p}) \equiv |\langle\Omega|\phi_R|n,\mathbf{p}\rangle|^2, \qquad (16)$$

which also will yield the "Bethe-Salpeter" amplitudes from which information about the structure of the pion can be extracted.

The data for the two-point function that correspond to the same absolute value of the spatial momentum are averaged per configuration. The different configurations are then combined in jackknife averages with a block size ranging from 1 to 5. No significant changes in the errors of the averages

---

[1]For definiteness we have taken $a = 0.105$ fm from [19] to set the scale.

(a)

(b)
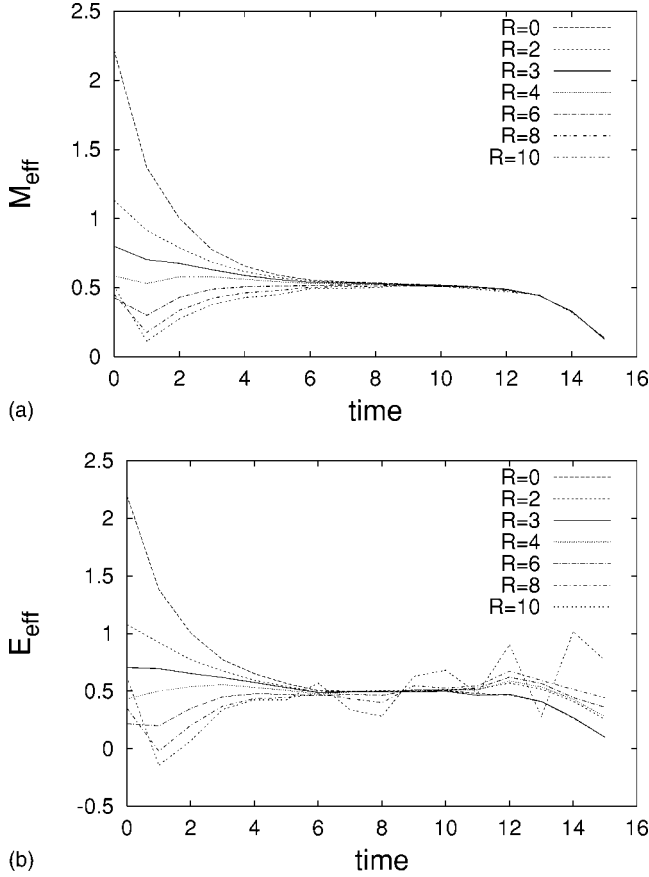
FIG. 4. Effective masses (a) and effective energies (b) for various R. In (a) the pion mass is $m_\pi = 970$ MeV; in (b) $m_\pi = 540$ MeV and $p^2 = 0.48$ GeV^2.

were observed for increasing block size, indicating that there are no significant correlations in our ensemble.

A. The fuzzing distance R

To determine the optimal value for the interquark distance R we used the jackknife averages to calculate the effective energy of the pion,

$$E_{\mathrm{eff}}(t,|\mathbf{p}|) = \ln[\langle G_{2,R}(t,\mathbf{p})\rangle/\langle G_{2,R}(t+1,\mathbf{p})\rangle]. \quad (17)$$

We varied R from 0 to 10, plotted the effective energy for these different fuzzing levels and looked which one stabilizes first. An example of the dependence on R is shown in Fig. 4(a) for the effective mass $M_{\mathrm{eff}}(t) = E_{\mathrm{eff}}(t,0)$, and for the effective energy in Fig. 4(b) with $|\mathbf{p}|^2 = 0.48$ GeV^2, corresponding to the momentum of the pion in our form factor extraction below. The optimal R value is somewhat dependent on the pion's momentum and mass. After several such tests, we chose $R=3$ as the common extension parameter for all calculations. Enhancing the ground state contribution is particularly important for the three-point function, where the distance between source and sink is typically small.

B. Pion masses and energies

Having chosen the fuzzing distance R, we extract the pion masses and energies by fitting the jackknife averages to Eq.
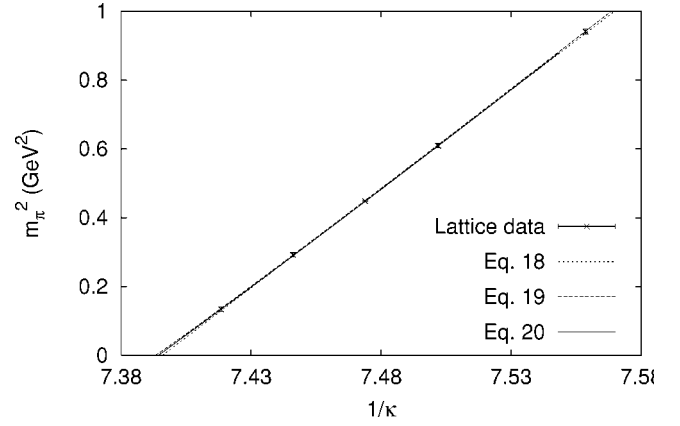
FIG. 5. Pion masses as functions of κ. Lines: extrapolations as indicated.

(15) for both a single state and two states. The fit range, the number of included time slices centered around the midpoint of our time grid at $t = 16$, is reduced until the minimum χ^2 is found and consistency between both fits can be checked. In extracting the masses from the $\mathbf{p}=\mathbf{0}$ averages, we found that for a single-state fit a fit range of about 15–17 time slices gives the lowest χ^2. In the case of a two-state fit, fitting the complete t range (31 time slices) yields the smallest statistical error; χ^2 per degree of freedom (DOF) is about the same for different fit ranges. We found consistency between the two fits. The resulting masses are given in Table I and plotted in Fig. 5 as a function of the inverse of the hopping parameter κ. They agree very well with the results obtained in, e.g., [22,23], whose authors use the same action as we do. Also shown are extrapolations to the chiral limit, based on the following fit functions:

$$m_\pi^2 = c_1\left(\frac{1}{\kappa} - \frac{1}{\kappa_c}\right) \quad (18)$$

$$m_\pi^2 = c_2\left(\frac{1}{\kappa} - \frac{1}{\kappa_c}\right)^{1/(1+\delta)} \quad (19)$$

and

$$\frac{1}{\kappa} = \frac{1}{\kappa_c} + b_1 m_\pi^2 + b_2 m_\pi^3, \quad (20)$$

resulting in a slightly different value for κ_c. Quenched chiral perturbation theory predicts the second form with δ small and positive [24]. As in [22], we obtain a negative value for δ. Equation (20) is a phenomenological fit [22]. There is no significant difference in the fit quality, so we cannot prefer one fit over the other. Therefore, we simply average the different values, yielding $\kappa_c = 0.13524(4)$, which agrees quite well with values obtained from the literature, $\kappa_c = 0.13531(1)$ [22] and $\kappa_c = 0.13525(1)$ [23]. The bare quark masses we obtain with our κ_c are given in Table I. They will be used in the (small) mass dependent correction of the improved current.

Proceeding analogously, we have also extracted the pion energies $E_{\mathbf{p}}^0$ for several nonvanishing three-momenta, again
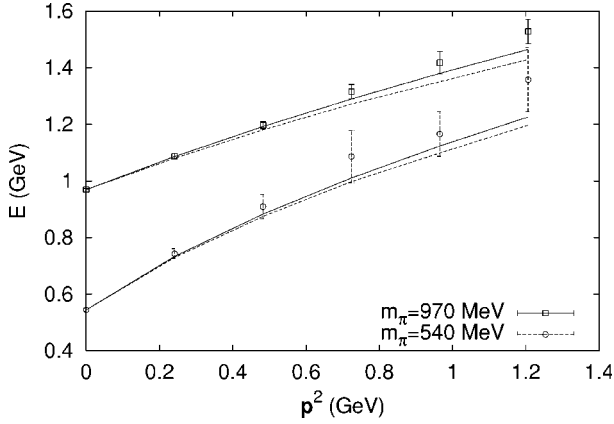
FIG. 6. Energy-momentum relation for $\kappa = 0.13230$ and 0.13430; solid line, continuum relation; dashed line, lattice dispersion relation.

using single- and two-state fits in combination. The results for the ground state energy are shown in Fig. 6, together with the prediction from the continuum dispersion relation,

$$E_{\text{cont}} = \sqrt{m_\pi^2 + \mathbf{p}^2},\tag{21}$$

and from the generally favored lattice dispersion relation,

$$\sinh^2 \frac{E}{2} = \sinh^2 \frac{M}{2} + \sum_{i=1}^{3} \sin^2 \frac{p_i}{2}.\tag{22}$$

The data deviate from both predictions at higher momenta. However, the figure clearly demonstrates that for the momentum relevant for our form factor extraction, $\mathbf{p}^2 = 0.48$ GeV^2, we are dealing essentially with continuum kinematics.

C. Results for the ρ mass

In the discussion of the form factor, we will often refer to the vector meson dominance model. For completeness and as a further test for our methods, we have also extracted the mass of the lowest vector meson, the ρ meson. Proceeding analogously as for the pion, Eq. (1), we consider a two-point function with source and sink operators of the form

$$V_i = \bar{\psi} \gamma_i \psi,\tag{23}$$

which project onto the polarization state i of a vector meson. With the same boundary conditions as for the pion, the two-point function for three-momentum $\mathbf{p} = \mathbf{0}$ was then fitted to a cosh form as in Eq. (15). We averaged the polarization states $i = 1,2,3$. The results for the three highest parameters κ are shown in Table I. They agree with the values obtained in [22,23]. For the remaining two κ values our statistics were not sufficient. When needed later for comparison with the vector meson dominance model for the form factor, we will for simplicity use the values from [22].
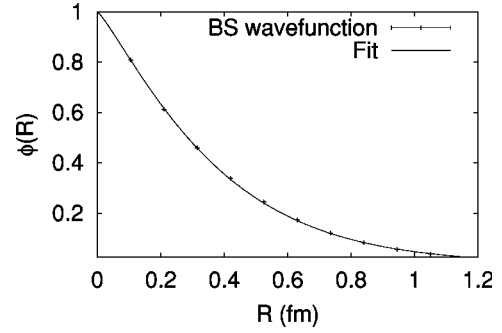
FIG. 7. BS wave function for $\kappa = 0.13230$.

D. Bethe-Salpeter amplitude and $\langle r^2 \rangle_{\text{BS}}$

To obtain the "Bethe-Salpeter (BS) amplitudes" or "wave functions" $\Phi(R)$, we use the Z factors extracted from a fit of the two-point function [Eq. (15)], since for a pion at rest

$$\Phi(R) = \sqrt{Z_R^0(\mathbf{0})/Z_0^0(\mathbf{0})}.\tag{24}$$

We simultaneously fitted the jackknife averages for R ranging from 0 to 10. Again the results from both the single- and a two-state parametrization were used to check the consistency.

The same results for the wave function, but with smaller errors, were obtained from a fit to the plateau of the ratio

$$\bar{\Phi}(R) = \frac{G_{2,R}(t,\mathbf{0})}{G_{2,0}(t,\mathbf{0})}.\tag{25}$$

An example of a BS wave function is shown in Fig. 7 for the heaviest pion; only the result of the second method is displayed. The wave function can be used to obtain an estimate of the mean square charge radius of the pion according to [4,5]

$$\langle r^2 \rangle_{\text{BS}} := \frac{1}{w} \frac{\int d^3 \vec{r}\, \vec{r}^2 \Phi^2(|\vec{r}|)}{\int d^3 \vec{r}\, \Phi^2(|\vec{r}|)}.\tag{26}$$

The factor w is included to reflect the uncertainty in the resulting $\langle r^2 \rangle$. If one assumes that the quark and antiquark are always located on opposite sides of the meson center of mass at distance $r/2$, one has $w = 4$; assuming that the quarks move in an uncorrelated way around the center of mass, $w = 2$ should be used. The BS radii as a function of the pion mass are given in Table I for $w = 2$. The values are much lower than the physical value of 0.439(8) fm^2 [25]. Moreover, the mean square radius is seen to be almost independent of the pion mass in the investigated range. We will comment on this in more detail in Sec. V.

IV. THE THREE-POINT FUNCTION

For the three-point function, already introduced in Sec. II, we now consider a pseudoscalar source at $t = 0$, a sink at $t_f = 11$, and a coupling to the photon at t with $0 < t < t_f$. Barad et al. [1] pointed out that current conservation provides an important numerical test which relates the two- and three-point functions. Translated into momentum space and for our

periodic boundary conditions, this relation reads

$$G_3(t_f,t;\mathbf{p},\mathbf{p}) - G_3(t_f,t';\mathbf{p},\mathbf{p}) = G_2(t_f,\mathbf{p}), \qquad (27)$$

where, in the second term on the left hand side (LHS), t_f $<t'<N_\tau$. This amounts to considering the total charge that leaves the source in the forward and backward direction in time and guarantees that $F(Q^2) = 1$ at $Q^2 = 0$. This relation holds for each background gauge field configuration separately and thus also for configuration averages. We have verified that our results for the conserved current satisfy this relation to an accuracy better than $O(10^{-5})$.

In order to obtain $F(0)$ for the renormalized local and the improved current, we again exploited Eq. (27). The LHS of this equation was averaged over pairs of values t and t' symmetric around t_f and normalized by the two-point function. Utilizing the Z_V factor from [20] gives $F^I(0)$ $= F^{\text{RL}}(0) = 1$ within a jackknife error of 1%. Alternatively, we could have applied this method to independently extract Z_V as done, e.g., in [26]. However, for consistency we used the entire set of improvement parameters from [20].

While the above method allows one to determine $F(0)$, we now describe how we extract the form factor for Q^2 >0. As in the two-point function we allow two states to contribute and parametrize the three-point function, Eq. (3), as

$$G_{3,\mu}(t_f,t;\mathbf{p}_f,\mathbf{p}_i) = \sum_{m=0}^{1} \sum_{n=0}^{1} \sqrt{Z_R^m(\mathbf{p}_f)Z_0^n(\mathbf{p}_i)}$$

$$\times \langle m,\mathbf{p}_f|j_\mu(0)|n,\mathbf{p}_i\rangle e^{-E_{\mathbf{p}_f}^m(t_f-t) - E_{\mathbf{p}_i}^n t}, \qquad (28)$$

where $(m,n) \neq (1,1)$. Contributions from, for example, the production of pion pairs, as well as "wraparound effects" due to the propagation of states beyond t_f are exponentially suppressed $[<O(e^{-5})]$; similarly, an elastic contribution from the excited state was estimated to be of the order of 1% or less. All these effects are not reflected in the chosen parameterization. The inelastic transitions $0\leftrightarrow1$ are included to better describe the data. However, it should be understood that the state labeled 1 parametrizes contributions from all possible excited states. Therefore we do not interpret our parameters as the energy or the transition form factors corresponding to a single genuine excited state.

Since for a given momentum the pion is the state with the lowest energy, one gets with Eqs. (9) and (10)

$$G_{3,\mu}(t_f,t;\mathbf{p}_f,\mathbf{p}_i)$$

$$= F(Q^2)\frac{(p_f+p_i)_\mu}{2\sqrt{E_{\mathbf{p}_f}^0 E_{\mathbf{p}_i}^1}}\sqrt{Z_R^0(\mathbf{p}_f)Z_0^0(\mathbf{p}_i)}e^{-E_{\mathbf{p}_f}^0(t_f-t)-E_{\mathbf{p}_i}^0 t}$$

$$+ \{\sqrt{Z_R^1(\mathbf{p}_f)Z_0^0(\mathbf{p}_i)}\langle 1,\mathbf{p}_f|j_\mu(0)|0,\mathbf{p}_i\rangle$$

$$\times e^{-E_{\mathbf{p}_f}^1(t_f-t)-E_{\mathbf{p}_i}^0 t} + (1\leftrightarrow 0)\}. \qquad (29)$$

In the simulations, we took $|\mathbf{p}_f| = |\mathbf{p}_i| = \sqrt{2}|\mathbf{p}_{\text{min}}|$, where

(a)

(b)
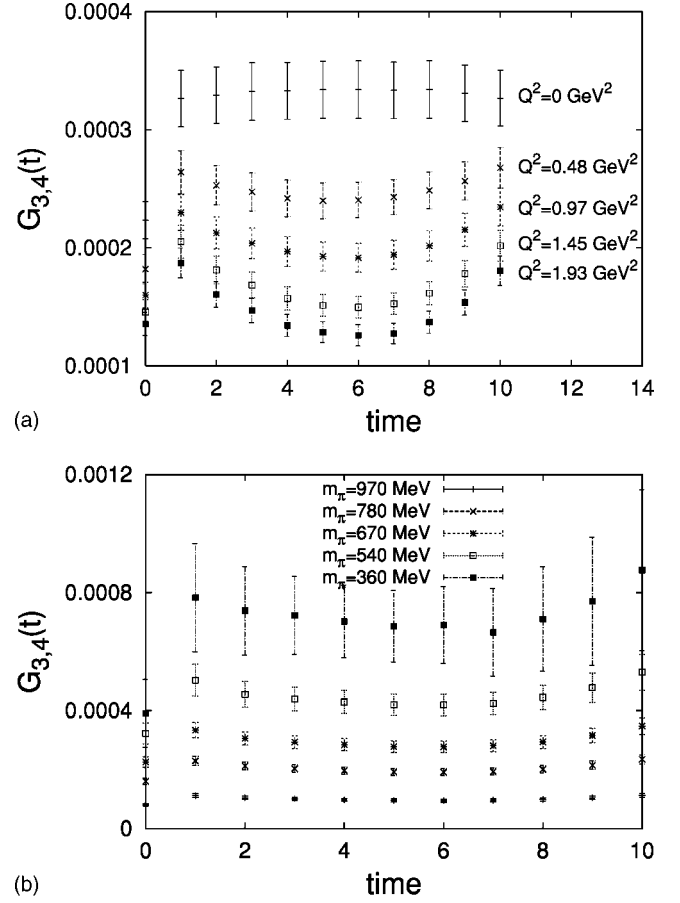
FIG. 8. Improved three-point function for (a) different Q^2 at $m_\pi = 780$ MeV and (b) different m_π at $Q^2 = 0.97$ GeV^2.

$$|\mathbf{p}_{\text{min}}| = \frac{2\pi}{N_\sigma a} \qquad (30)$$

is the minimal momentum for a lattice with N_σ lattice points in the spatial extension. In our case, it amounts to

$$\mathbf{p}_i^2 = \mathbf{p}_f^2 = 0.48 \quad \text{GeV}^2. \qquad (31)$$

For our analysis we use the fourth component of the current, $\mu = 4$. With our choice of momenta the kinematical factors in the fit function Eq. (29) therefore simplify considerably [see Eq. (13)]; note also that the t dependence of the first term in Eq. (29) vanishes. As a result, the form factor is more easily extracted without restricting the simulation too much. Different momentum transfers are obtained by varying the relative orientation of $\mathbf{p}_i$ and $\mathbf{p}_f$.

A. Extraction of parameters

We begin by averaging the three-point correlation functions which have the same four-momentum transfer squared and then again combine the configurations in jackknife averages. Typical jackknife averages of the three-point function are shown in Fig. 8(a) for the next highest pion mass for various momentum transfers and for different masses at fixed momentum transfer in Fig. 8(b). If only the pion ground state

contributed, there would be no t dependence in this quantity. The data, however, clearly indicate the admixture of an excited state. This is especially seen at high Q^2 and for low pion masses, where there is no time slice where it is safe to assume that only the pion ground state is present.

We therefore chose to proceed by simultaneously fitting the parameters in the two-point and three-point functions, Eqs. (15) and (29), respectively. We hereby exploit the fact that certain parameters appear in both Green's functions. In the case of the two-point function, we fitted the energies E^0 and E^1 and the Z factors over the complete time interval $1 \leq t \leq N_\tau - 1$. In the three-point function, we fit the same energies and Z factors, and in addition the form factor $F(Q^2)$ and the transition matrix elements over the interval $t_i < t < t_f$. We assume that the energies and Z factors depend only on the magnitude of the three-momenta and use the fact that we chose $|\mathbf{p}_f| = |\mathbf{p}_i|$. The fits are done for each value of Q^2 separately. The values for χ^2/DOF lie between 0.15 and 0.40, depending on mass and momentum transfer. The energies and Z factors we obtain from our fits at different Q^2 agree to high accuracy because they are largely determined by the two-point function.

To compare with earlier work [10,11] we also extracted an estimate for the form factor from the ratio of three- and two-point functions. However, the assumption of just a single state contributing is at the basis of this method. Correspondingly, we found differences ranging from 5 to 10 % for $F(Q^2)$ between the ratio method and our combined fit method, where inclusion of an excited state clearly improved the fit quality. The size of the difference depends on the pion mass and the momentum transfer, which influences the flatness of the three-point function in the middle between source and sink. All our results in the next section are therefore based on the fit method.

V. RESULTS AND DISCUSSION

We will now discuss the form factors obtained from the procedure described in the previous section.

A. Dependence on the current

We first compare the form factors we obtain with the local current Eq. (4), the conserved current Eq. (5), and the improved current Eq. (6). Only the improved current ensures that there are no corrections to $O(a)$ with our action.

The form factors for $Q^2 > 0$, obtained through the simultaneous fit procedure, are shown in Figs. 9(a) and 9(b) for two different masses. As can be expected from Fig. 8(a), the same fit procedure yields values for $F(0)$ with an error comparable to the results for low Q^2. However, we use the method discussed in connection with Eq. (27) to extract $F(0) = 1$ to higher accuracy.

We first of all observe that, as expected, the results for our heaviest pion, $m_\pi = 970$ MeV, are much more accurate than for the lightest pion, $m_\pi = 360$ MeV. However, even with the larger error bars, a rather smooth Q^2 dependence is seen also in the latter case. We further observe that the differences between the conserved and improved currents grow with in-

(a)

(b)
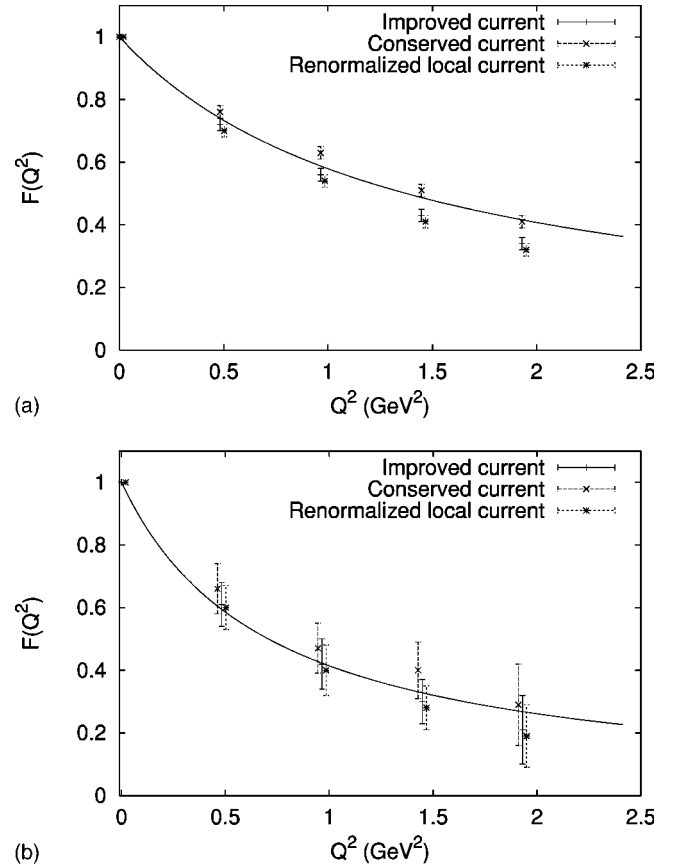
FIG. 9. Form factors extracted from different currents as a function of Q^2 for two pion masses: $m_\pi = 970$ (top) and 360 MeV (bottom). Solid curve: VMD model prediction with $m_V = m_\rho$ taken from [22]. Data shifted horizontally for clarity.

creasing momentum transfer and decreasing mass, resulting, in particular for the light pion mass, in a substantial correction. The differences between the improved and the renormalized local currents are due to the tensor term. Although this contribution increases with Q^2 the improved form factor stays very close to the result for the renormalized local current; also for the light pion and out to our largest momentum transfer. That these two form factors are so close is due to the fact that the contribution of the tensor term in the improved current is small. Since the matrix element of the tensor operator can become comparable in size (up to 70%) with the local current operator, this smallness is due to the fact that the coefficient $c_V = -0.107$ determined in [20] is rather small; the preliminary value obtained by the ALPHA Collaboration [15] is much larger, $c_V = -0.32$. Since the improved current is a linear combination of the local and the tensor term, Eq. (7), the change in the improved current due to a change in c_V is straightforward. The difference between the two values of c_V is of order a, resulting in improved currents which are different only at order a^2. This shows that $O(a^2)$ effects can still become as large as 10% at higher Q^2 values and low masses.

B. The form factor and vector meson dominance

As was already observed in [11], the lattice results for the form factor show a behavior expected from vector meson
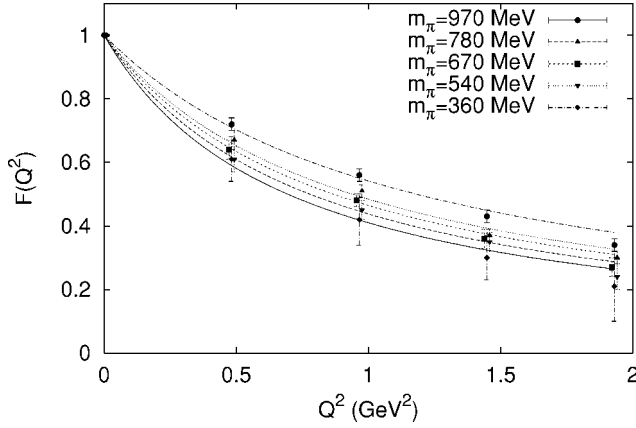
FIG. 10. Improved form factor as a function of Q^2 for different m_π. Lines: fits to VMD form Eq. (14).

dominance. In Figs. 9(a) and 9(b), we show the prediction for the form factor if we use the simple monopole form Eq. (14), with $m_V = m_\rho$, the lattice ρ mass at the same κ value [22]. At large pion mass the VMD prediction describes the form factor based on the conserved current rather well but lies substantially above the results from the improved current. However, at lower pion masses the model prediction shifts toward the improved form factor results. To investigate this point in more detail, we fitted the improved form factors, using the vector meson mass m_V as a fit parameter, omitting the point at the highest Q^2 value. The parametrization works well and results are shown in Fig. 10. Table II compares the fitted m_V values to the ρ mass extracted from two-point functions [22]. The two values can be seen to come closer together as the pion becomes lighter, suggesting a better agreement of the improved results with the simple vector meson dominance model for lower pion masses. However, as we will see later, in the physical limit, using $m_V = m_\rho$ fails to describe the experimental data accurately.

C. Determination of the charge radius

It is well known that the slope of the form factor is related to the mean square charge radius of the pion,

$$\left. \frac{\partial F(Q^2)}{\partial Q^2} \right|_{Q^2=0} = \frac{1}{6} \langle r^2 \rangle. \qquad (32)$$

In contrast to the charge radius extracted from the Bethe-Salpeter amplitude, this determination of $\langle r^2 \rangle$ is not based on

TABLE II. m_ρ from the two-point function [22], fitted m_V, and $\langle r^2 \rangle$ for different m_π values.

m_π (MeV)	m_ρ (MeV)	m_V (MeV)	$\langle r^2 \rangle$ (fm²)
970(4)	1169(3)	1086(26)	0.197(9)
780(4)	1032(4)	968(26)	0.249(13)
670(4)	966(6)	931(26)	0.269(15)
540(6)	901(6)	882(36)	0.299(24)
360(9)	841(24)	833(75)	0.34(6)
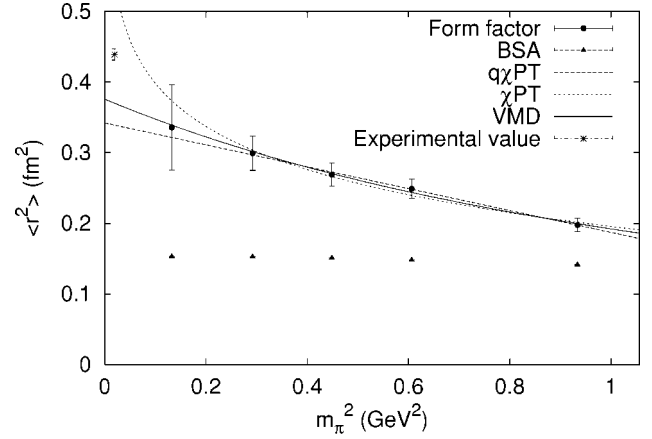
FIG. 11. Pion charge radii extracted from the form factor and extrapolations in m_π^2. The BS radii are included for comparison. Experimental result from [25].

any specific assumptions about the quark motion inside the pion. As the vector meson dominance model works very well for low Q^2, we show for simplicity the mean square charge radius of the pion obtained from the monopole fit, which yields

$$\langle r^2 \rangle = \frac{1}{m_V^2}. \qquad (33)$$

In the following we work only with the improved current. By looking at the values in Table II and in Fig. 11, we observe that the $\langle r^2 \rangle$ extracted from the form factor shows a considerable mass dependence. This is in contrast to the BS results, which are also shown. Moreover, these results, which we obtained in Sec. III D, are considerably lower than the value we extract from the form factor. As already discussed by Gupta *et al.* [6], this can be due to how one treats the center of mass of the two quarks. However, as these authors also point out, the value extracted through the form factor contains contributions that are not included when calculating $\langle r^2 \rangle$ from the Bethe-Salpeter amplitude.

The $\langle r^2 \rangle$ values obtained from the form factor can be seen to get closer to the physical value of $\langle r^2 \rangle = 0.439(8)$ fm² as the pion mass decreases. This led us to try several extrapolations to the physical limit which will be described in the next section.

In addition to the two methods discussed above, there is another method to obtain the charge radius of the pion from lattice QCD. This method is based on calculating density-density correlations or four-point functions for the pion [1,8]. It has recently been used by Alexandrou *et al.* [9] for densities at equal times. However, there are difficulties in the extraction of $\langle r^2 \rangle$ from density-density correlations as discussed in detail by Burkardt *et al.* [27] and Wilcox [28].

D. Extrapolation in m_π

To obtain more physical results, one can try to extrapolate in the pion mass. We take $\langle r^2 \rangle$ as the quantity to extrapolate, since it is known experimentally and its extrapolation has
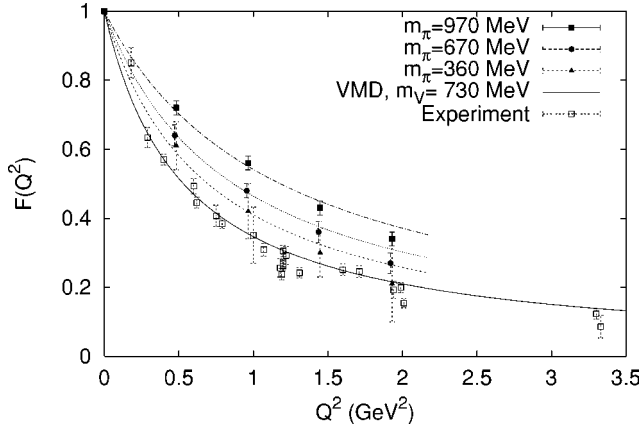
FIG. 12. Improved form factor for different m_π, compared to experiment [32,33]; broken lines as in Fig. 10.

been discussed in the literature. We consider three different types of extrapolations. From chiral perturbation theory (χPT), one knows the one-loop result [29],

$$\langle r^2 \rangle_{\chi PT}^{one\ loop} = c_1 + c_2 \ln m_\pi^2. \tag{34}$$

In our fit, we will treat c_1 and c_2 as free parameters. In *quenched* χPT (QχPT), the radius is constant at this order of expansion [30]. It is, however, expected that this situation will change at the two-loop level, which will introduce terms like

$$\langle r^2 \rangle_{Q\chi PT}^{two\ loop} \sim d_1 \frac{1}{m_\pi^2} + d_2 \ln m_\pi^2 + d_3 m_\pi^2, \tag{35}$$

including a term linear in m_π^2 which, for our pion masses, can be expected to yield the dominant contribution [31]. We therefore tried only a form containing a constant plus a term linear in m_π^2.

We have observed that our form factor data can be well described by a monopole form as suggested by simple vector meson dominance. Therefore, we use this model to obtain an additional extrapolation. Since it can be seen that m_V, just like m_ρ, scales approximately linearly with m_π^2, one arrives at

$$\langle r^2 \rangle_{VMD} = \frac{6}{(b_1 + b_2 m_\pi^2)^2}. \tag{36}$$

The three extrapolations are plotted in Fig. 11. The extrapolated value is seen to depend strongly on the method chosen. The VMD ansatz describes the data best. If we use this ansatz to extrapolate to the physical pion mass we find $\langle r^2 \rangle = 0.37(2)$ fm^2, which lies below the experimental value of $0.439(8)$ fm^2. This could clearly be due to the extrapolation chosen, but also due to assumptions and approximations, such as quenching, inherent in our approach.

E. Comparison with experiment

In Fig. 12 we show our results together with the available measurements [32,33]. For clarity we show only our results

for three κ values. As can be clearly seen, all our calculated form factors lie above the measured values. Nevertheless, a continuous trend toward the experimental values can be observed and we come quite close to them. Whether only a straightforward further lowering of the pion mass will resolve the remaining discrepancy between our lattice calculations and experiment is not clear. The solid line in the figure shows the monopole form using $m_V^2 = 6/\langle r^2 \rangle_{expt}$ with the experimentally measured charge radius $\langle r^2 \rangle_{expt}$. This also describes the experimental data quite well away from $Q^2 = 0$. However, the corresponding vector meson mass at 730 MeV is significantly lower than the ρ mass, emphasizing that the VMD inspired monopole description provides a successful parametrization of the form factor data but does not hold in detail.

VI. SUMMARY AND CONCLUSIONS

We have presented calculations for the pion form factor that improved and extended previous work in several respects. We have pushed the form factor calculations for a large range of Q^2 toward much lower pion masses than before. In doing this, we have worked in a framework that guarantees the absence of $O(a)$ corrections. This meant a consistent use of an improved action with the concomitant improved conserved current. It was shown that use of this improved current leads to significant changes over results based on the conserved Noether current for this action, which still contains $O(a)$ corrections at finite Q^2. We chose kinematics where the initial and final pion momenta had the same absolute value, which leads to practical simplifications when extracting the form factor. For the momenta we use, we confirmed that energy and momenta are sufficiently close to satisfying a continuum dispersion relation.

Our results for the form factor were seen to smoothly vary with pion mass. The lower Q^2 results could all be described quite well by a simple monopole form factor. The fitted range parameter m_V^{-1} was, for each κ value, found to be close to the corresponding lattice ρ mass. The agreement between the two values got closer for decreasing pion mass, indicating better agreement with the vector meson dominance model.

The form factor can be used to extract the mean square charge radius of the pion. The values we obtained show that the estimates for $\langle r^2 \rangle$ based on the Bethe-Salpeter amplitude are qualitative as well as quantitative not very reliable. Disagreement of up to a factor 2 was found with the form factor based values, which showed also a quite pronounced mass dependence in contrast to the BS results. Extrapolations of our charge radii toward the physical pion mass were shown to lead to no unique prediction. The best description of the results at our pion masses was provided by a vector meson dominance model. When extrapolated to the physical pion mass, it yields a value for $\langle r^2 \rangle$ about 15% below the experimental value. For an extrapolation inspired by (quenched) chiral perturbation theory our pion masses are too high to be sufficiently sensitive to the predicted $\ln m_\pi^2$ terms.

When compared to the experimental form factor, it could be seen that our results consistently approach the data from

above over the entire range of Q^2 we consider. While gauge invariance fixes all form factors at $Q^2 = 0$ to $F(0) = 1$, we see that the calculated form factor at $Q^2 > 0$ comes close to the experimentally determined shape, and to a monopole parametrization. This is a nice confirmation that lattice QCD indeed describes a nonperturbative feature such as a pion form factor quite realistically and in detail. However, a straightforward extension of our approach to even lower pion masses or higher Q^2 is not necessarily the way to proceed to close the last gap with the experiment. Improvements of our approach and other lattice methods will become necessary. Corrections of order $O(a^2)$, for example, will become increasingly important and one also has to understand the role of dynamical quarks, which are neglected in the quenched approximation.

As is well known, Wilson fermions have the major disadvantage that chiral symmetry is already broken at $O(a)$. This was one of the reasons improvement was invented and why we chose a framework where action and operators were consistently improved and corrections only to order $O(a^2)$ show up. Another method, among others, is the introduction of a fifth dimension and use of so-called domain wall fermions. Chiral symmetry is then not tied to taking the continuum limit. The price one pays is a substantial increase in the computer time. The RBC Collaboration has chosen this approach and first results can be found in [34]. In this paper pion masses down to 390 MeV are used, albeit on a coarser lattice. Their results obtained so far at two low Q^2 points,

based on the renormalized local current, seem to agree reasonably well with our values. Differences in the implementation of chiral symmetry show up at $O(a^2)$.

An open question is of course the significance of the quenched approximation. Alexandrou *et al.* [9] have calculated density-density correlations for the π, ρ, N, and Δ in quenched as well as unquenched lattice QCD. In contrast to the ρ and Δ, only rather small effects are seen for the π for values of m_π around 600 MeV. The study of effects due to dynamical quarks, clearly more important at lower pion masses and high Q^2, is an area where further work is necessary.

ACKNOWLEDGMENTS

[1] K. Barad, M. Ogilvie, and C. Rebbi, Phys. Lett. **143B**, 222 (1984).

[2] J. van der Heide, M. Lutterot, J. H. Koch, and E. Laermann, Phys. Lett. B **566**, 131 (2003).

[3] J. van der Heide, hep-lat/0309183.

[4] M. W. Hecht and T. A. DeGrand, Phys. Rev. D **46**, 2155 (1992).

[5] E. Laermann and P. Schmidt, Eur. Phys. J. C **20**, 541 (2001).

[6] R. Gupta, D. Daniel, and J. Grandy, Phys. Rev. D **48**, 3330 (1993).

[7] M.-C. Chu, M. Lissia, and J. W. Negele, Nucl. Phys. **B360**, 31 (1991).

[8] W. Wilcox and K.-F. Liu, Phys. Lett. B **172**, 62 (1986).

[9] C. Alexandrou, P. de Forcrand, and A. Tsapalis, Phys. Rev. D **66**, 094503 (2002).

[10] G. Martinelli and C. T. Sachrajda, Nucl. Phys. **B306**, 865 (1988).

[11] T. Draper, R. M. Woloshyn, W. Wilcox, and K.-F. Liu, Nucl. Phys. **B318**, 319 (1989).

[12] L. H. Karsten and J. Smit, Nucl. Phys. **B183**, 103 (1981).

[13] G. Martinelli, C. T. Sachrajda, and A. Vladikas, Nucl. Phys. **B358**, 212 (1991).

[14] M. Lüscher, S. Sint, R. Sommer, and H. Wittig, Nucl. Phys. **B491**, 344 (1997).

[15] M. Guagnelli and R. Sommer, Nucl. Phys. B (Proc. Suppl.) **63**, 886 (1998).

[16] K. Fabricius and O. Haan, Phys. Lett. **143B**, 495 (1984); A. D. Kennedy and B. J. Pendleton, *ibid.* **156B**, 393 (1985).

[17] B. Sheikholeslami and R. Wohlert, Nucl. Phys. **B259**, 572 (1985).

[18] M. Lüscher, S. Sint, R. Sommer, P. Weisz, and U. Wolff, Nucl. Phys. **B491**, 323 (1997).

[19] R. G. Edwards, U. M. Heller, and T. R. Klassen, Nucl. Phys. **B517**, 377 (1998).

[20] T. Bhattacharya, R. Gupta, W.-J. Lee, and S. R. Sharpe, Phys. Rev. D **63**, 074505 (2001).

[21] UKQCD Collaboration, P. Lacock, A. McKerrell, C. Michael, I. M. Stopher, and P. W. Stephenson, Phys. Rev. D **51**, 6403 (1995).

[22] M. Göckeler *et al.*, Phys. Rev. D **57**, 5562 (1998).

[23] UKQCD Collaboration, K. C. Bowler *et al.*, Phys. Rev. D **62**, 054506 (2000).

[24] S. R. Sharpe, Nucl. Phys. B (Proc. Suppl.) **30**, 213 (1993).

[25] NA7 Collaboration, S. R. Amendolia *et al.*, Nucl. Phys. **B277**, 168 (1986).

[26] QCDSF-UKQCD Collaboration, T. Bakeyev *et al.*, Phys. Lett. B **580**, 197 (2004).

[27] M. Burkardt, J. M. Grandy, and J. W. Negele, Ann. Phys. (N.Y.) **238**, 441 (1995).

[28] W. Wilcox, Phys. Rev. D **66**, 017502 (2002).

[29] J. Gasser and H. Leutwyler, Ann. Phys. (N.Y.) **158**, 142 (1984).

[30] G. Colangelo and E. Pallante, Nucl. Phys. **B520**, 433 (1998).

[31] C. Colangelo (private communication).

[32] C. J. Bebek *et al.*, Phys. Rev. D **17**, 1693 (1978).

[33] Jefferson Lab F(pi) Collaboration, J. Volmer *et al.*, Phys. Rev. Lett. **86**, 1713 (2001).

[34] RBC Collaboration, Y. Nemoto, hep-lat/0309173.